Ozonization at the Vacancy Defect Site of the Single-Walled Carbon Nanotube

Lei Vincent Liu, Wei Quan Tian,† and Yan Alexander Wang*

Department of Chemistry, University of British Columbia, Vancouver, BC V6T 1Z1, Canada

Received: October 19, 2005; In Final Form: April 26, 2006

The ozonization at the vacancy defect site of the single-walled carbon nanotube has been studied by static quantum mechanics and atom-centered density matrix propagation based ab initio molecular dynamics within a two-layered ONIOM approach. Among five different reaction pathways at the vacancy defect, the reaction involving the unsaturated active carbon atom is the most probable pathway, where ozone undergoes fast dissociation at the active carbon atom at 300 K. Complementary to the experiments, our work provides a microscopic understanding of the ozonization at the vacancy defect site of the single-walled carbon nanotube.

1. Introduction

Single-walled carbon nanotubes (SWCNTs) have been intensively studied during the past decade since the discoveries of Iijima in the early 1990s.[1] A lot of potential applications of the SWCNTs have been proposed due to their unique properties: high Young's modulus, high thermal conductivity, and high aspect ratio structure, etc. Over the years, applications of the SWCNTs have been successfully realized as chemical sensors,[2] hydrogen storage materials,[3] and vacuum electronic devices.[4] Access to the interior of the SWCNTs is essential for most of these applications.

Unfortunately, most of the SWCNTs are synthesized with closed hemispherical fullerenelike end-caps, which prevent internal adsorption of chemical reagents.[5] It is thus often necessary to open the capped ends via chemical means,[6−14] which take advantage of the higher reactivity of the end-caps. Such a higher reactivity is a result of the fact that the pyramidalization angles of any hemispherical fullerenelike end-caps are bigger than those of the sidewalls of the nanotubes. Gas-phase ozone oxidation is one of the well-developed end-opening methods.[9−13] The oxidation process removes the caps and introduces or enlarges vacancy defects on the sidewall, producing two kinds of functional groups, esters and quinones, at the ends or at the defective sites of the sidewall.[9−13] After high-temperature thermal treatment, these two functional groups will decompose and emit a large amount of CO and CO_2.[11−13]

Olefin ozonolysis can be understood through the standard Criegee's mechanism[15] (Scheme 1). As an 18-valence-electron, 1,3-dipolar molecule, ozone (**2**) reacts with an olefin (**1**) via the 1,3-dipolar cycloaddition (1,3-DC) to the π bond of the olefin and forms the primary ozonide (**3**), which has an unstable five-membered ring. The C−C single bond and one of the O−O bonds of the primary ozonide then break to produce a carbonyl compound (**5**) and a carbonyl oxide (**6**) in a zwitterion form. These two compounds (**5** and **6**) will recombine to form an ozonide (**7**). Recently, a similar Criegee's mechanism has been proposed in the reactions of ozone with C_{60} and the SWCNTs.[16−18]

Several theoretical studies have been carried out to understand the ozonization of the perfect SWCNTs[17,18] and the SWCNTs with Stone-Wales defects.[19−21] To the best of our knowledge, there has been no reported theoretical studies on the chemical reaction of ozone with the vacancy defect sites of the SWCNTs. Vacancy defects can either occur as native defects or be induced by ion or electron irradiation of the SWCNTs.[22,23] The structures, mechanical and electronic properties, and potential applications of the SWCNTs with vacancy defects have been recently predicted theoretically.[23−30] Direct observations of the vacancy defects on graphite and double-walled carbon nanotubes have been reported recently by Iijima and co-workers using in situ high-resolution transmission electron microscopy technique.[31,32] In our previous studies, we have shown that the vacancy defect introduces localized electronic states at the defect site, which leads to regioselectivity on the sidewall and further facilitates the selective functionalization of the SWCNTs.[25−27] Such reactivity of the vacancy defect was utilized to cut the SWCNTs in a well-controlled oxidative way by Smalley and co-workers,[33] recently.

In this work, we present our theoretical studies of the ozonization at the single vacancy defect site on the sidewall of the (5,5) SWCNT to further understand the chemical properties of the vacancy defect site. We anticipate a similar reactivity of the vacancy defects on the outmost layer of the multiwalled carbon nanotubues (CNTs), because the large interlayer distance makes the chemical effect of the inner CNTs on the outmost CNT unlikely. Moreover, the chirality of the SWCNT should have a more important effect on the reactivity of the vacancy defect than the diameter of the SWCNT, since the chirality of the SWCNT can readily modify the structure of the vacancy defect.[24] It is our hope that our studies will make the first step toward the comprehensive understanding of the chemistry of the vacancy defect site of CNTs of various forms.

2. Computational Methods

We first built a fragment of the (5,5) SWCNT of 120 carbon atoms with 20 end-capping hydrogen atoms, $C_{120}H_{20}$. The hydrogen atoms are used to saturate the carbon atoms with dangling bonds at the two ends. We then removed one carbon atom from the middle of the sidewall of $C_{120}H_{20}$, producing an ideal single vacancy, which contains three carbon atoms with dangling bonds (Figure 1a). Due to the large system size, we first employed the semiempirical AM1 method[34] to optimize the geometry. We further refined the AM1 optimized geometry with density functional theory (DFT) at the B3LYP/6-31G(d)

* Corresponding author. E-mail: yawang@chem.ubc.ca.

† Current address: Department of Material Sciences, Faculty of Engineering Sciences, Kyushu University, 6−1 Kasugakoen, Kasuga, Fukuoka, 816-8580, Japan.

10.1021/jp055999x CCC: $33.50
Published on Web 06/14/2006

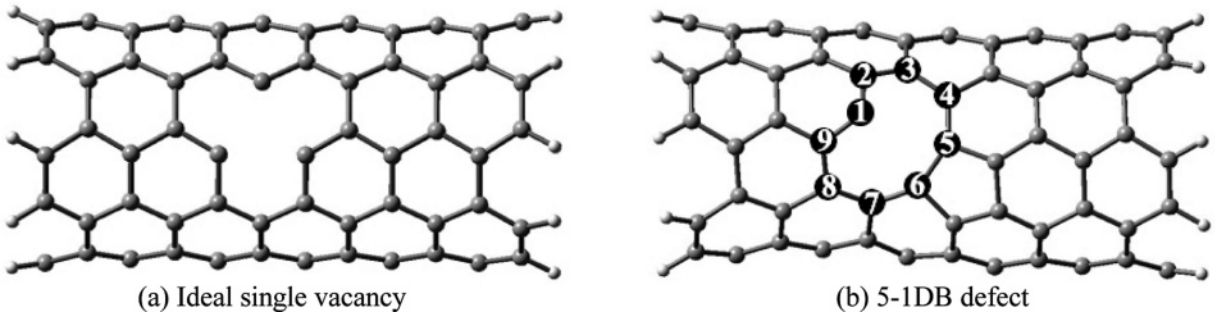

Figure 1. Single vacancy defect on the sidewall of the (5,5) SWCNT (carbon atoms within the nine-membered ring of the 5-1DB defect are numbered). (a) Ideal single vacancy. (b) 5-1DB defect.

SCHEME 1: Criegee's Mechanism of Olefin Ozonolysis

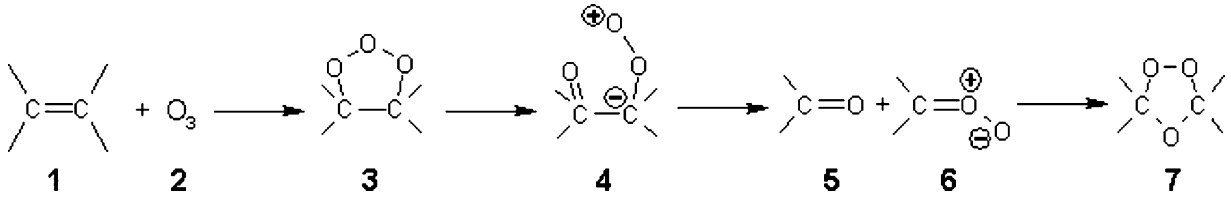

level of theory.[35,36] In the optimized structure, two of the three carbon atoms with dangling bonds combine to form an asymmetric 5-1DB defect,[23] which has one newly formed five-membered ring and one carbon atom with dangling bond (Figure 1b). We have carried out systematic theoretical calculations to examine the structure and the stability of the 5-1DB defect on the SWCNT and found that the ground state of the 5-1DB defect on the (5,5) SWCNT is singlet.[25−27,37]

We employed the ONIOM method[38] to explore the reaction pathways. In the ONIOM model, the AM1 method and the B3LYP/6-31G(d) method have been used for the lower- and higher-level treatments, respectively. The nine-membered ring of the 5-1DB defect was chosen to be the higher layer (Figure 1b). In fact, this is the only logical way to define the higher layer of the ONIOM model, because the nine-membered ring connects to its neighboring carbon atoms in the SWCNT via C−C single bonds, which are ideal to be replaced by buffering C−H single bonds in the ONIOM model. Incorporating more neighboring carbon atoms around the nine-membered ring into the expanded higher layer of the ONIOM model will inevitably cut many aromatic C=C double bonds, hence changing the electronic structure of the SWCNT.[26] This two-layered ONIOM model is capable of capturing the essential chemical reactivity of the 5-1DB defect.[26,27]

All of the structures of transition states, intermediates, and products were located by this two-layered ONIOM model. The Hessian was calculated to verify the nature of the stationary points on the potential energy surface: one and only one imaginary frequency for transition state and no imaginary frequency for the minima. Local minima connected by a transition state were found from the optimization of the disturbed structures of the transition state. To verify the results of the two-layered ONIOM model, single-point calculations were performed at the B3LYP/6-31G(d) level of theory whenever necessary.[26,27] Partial charges and bonding properties were studied by using the NBO 3.1[39] module in the Gaussian 03 package.[40]

Although, in the conventional quantum chemistry picture, O_3 and O_2 are both inherently multiconfigurational species, it has been well established that DFT is able to accurately treat such systems due to the incorporation of the exchange-correlation effects in the exchange and correlation functionals.[17,18,21,41] For singlet O_3, DFT calculations with the open-shell and closed-shell methodologies always converge to the closed-shell case. For O_2, we have adopted the restricted-open-shell methodology in the DFT calculations. We did not use the unrestricted method to describe open-shell O_2 species, because the unbalanced spin-contamination of the unrestricted method might yield unreasonable energy profiles. Moreover, in this research, we are only interested in the stationary points involving O_3 and O_2 rather than their dynamical scattering crossing sections on the potential energy surfaces; we are confident about our DFT description of the system investigated herein.

To confirm the assessment of the static quantum mechanical calculations, we also carried out the atom-centered density matrix propagation (ADMP)[42−45] based ab initio molecular dynamics (AIMD) to study the reaction of ozone with the vacancy defect site at 300 K with a time step 0.25 fs and a fictitious electronic mass of 0.1 au. A two-layered ONIOM/ADMP scheme was applied for the AIMD simulation.[46] The partition of the ONIOM model in the ADMP calculations is the same as that of the static quantum mechanical calculations, except that we used the universal force field (UFF)[47] for the lower layer to save computational time.

All the above calculations were carried out by using the Gaussian 03 package.[40]

3. Results and Discussion

3.1. Static Quantum Mechanical Studies. The bond lengths, bond orders, and partial charges of the nine-membered ring of the 5-1DB vacancy defect are shown in Table 1. Among these nine C−C bonds, the C5−C6 bond on the pentagon is the longest (with a bond length of 1.55 Å) and the weakest (with a bond order of 1.09). The C9−C1 bond is the shortest with a bond length of 1.39 Å and a bond order of 1.31. The carbon atom with the dangling bond, C1, has the largest positive charge, 0.10, whereas its two neighboring carbon atoms have the two largest negative charges, −0.12 for C2 and −0.05 for C9. These large partial charges significantly make the two bonds connecting C1 to its two neighboring carbon atoms C2 and C9 shorter and stronger. Previously, we have found that C1 is the major contributor to the highest occupied molecular orbital (HOMO) and the lowest unoccupied molecular orbital (LUMO) of the

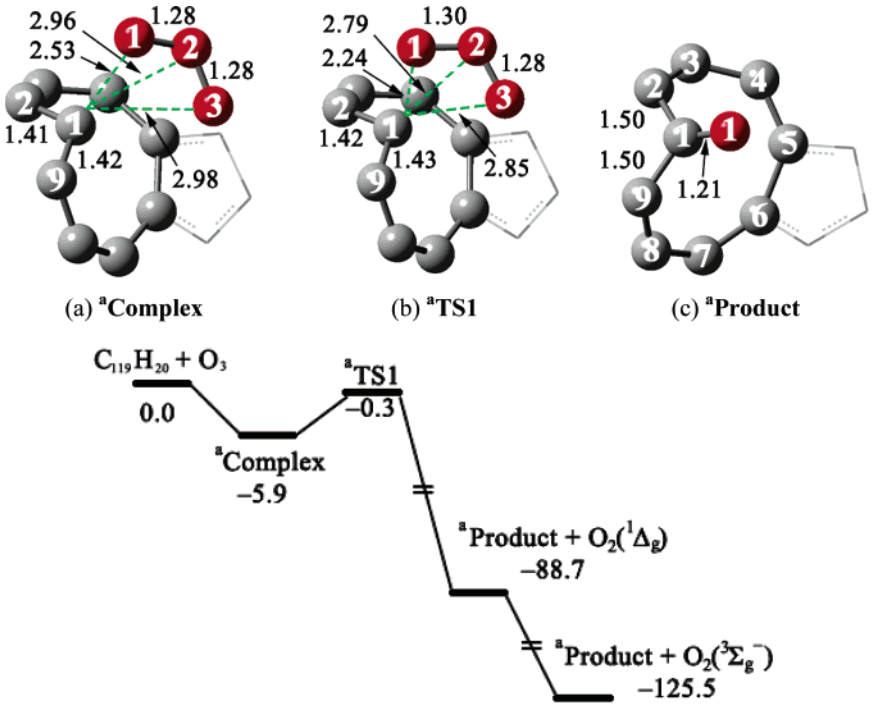

Figure 2. Geometries of the transition states, the intermediates, and the final product of the reaction of O_3 with the active carbon atom of $C_{119}H_{20}$. The units of energy and bond length are kcal/mol and Å, respectively. The oxygen atoms are in red.

TABLE 1: Bond Lengths (in Å), Bond Orders, and Partial Charges of the Nine-Membered Ring of the 5-1DB Defect

bond	bond length	bond order	atom	charge
C1−C2	1.40	1.31	C1	0.10
C2−C3	1.41	1.23	C2	−0.12
C3−C4	1.44	1.18	C3	0.03
C4−C5	1.46	1.27	C4	0.00
C5−C6	1.55	1.09	C5	0.01
C6−C7	1.44	1.35	C6	0.00
C7−C8	1.47	1.16	C7	0.00
C8−C9	1.42	1.28	C8	−0.03
C9−C1	1.39	1.31	C9	−0.05

vacancy-defected SWCNT.[26,27] The out-of-plane geometry and the large positive charge of C1 make it more reactive toward the attacking reagents. Hereafter, we will call C1 the active carbon atom.

The bond lengths and the bond orders indicate that around the 5-1DB defect site, the C2−C3, C4−C5, C6−C7, and C8−C9 bonds have some significant π bond character. In fact, these four bonds have similar bond lengths to the other aromatic C=C double bonds on the sidewall of the SWCNT. We, thus, studied the attacking of ozone on C1 and these four bonds in the nine-membered ring as prototype reactions of O_3 with the 5-1DB defect site, whose results are presented as the following: the reaction on C1, on the C8−C9 bond (position 1), on the C6−C7 bond (position 2), on the C4−C5 bond (position 3), and on the C2−C3 bond (position 4). At the end, we present our ADMP results to further verify the conclusions derived from the static modeling.

3.1.1. Reaction of O_3 on the Active Carbon Atom. The structures of the initial intermediate ([a]Complex) and the initial attacking transition state on C1 ([a]TS1) are shown in Figure 2a and b. In [a]Complex, O_3 and C1 form a four-membered ring. On the basis of the NBO analysis of [a]Complex, the partial charges of C1, O1, O2, and O3 are 0.13, −0.20, 0.23, and −0.21, respectively, which means that 0.19 electrons are transferred from the SWCNT to O_3. In terms of electrostatic effects, the electrostatic attractions between C1 and O1 and between C1 and O3 stabilize [a]Complex, whereas the electrostatic repulsion between C1 and O2 counteracts with this attractive stabilization. In [a]TS1, O_3 and C1 form a more compact four-membered ring than the one in [a]Complex. The bond lengths of the C1−O1 and C1−O3 bonds shorten to 2.24 and 2.85 Å, respectively. The imaginary vibrational mode shows the shortening of the C1−O1 bond and the elongating of the O1−O2 bond, indicating the attack of O1 to C1 and the breaking of the O1−O2 bond, i.e., the dissociation of O_3. On the basis of the NBO analysis of [a]TS1, the partial charges of O1, O2, O3, and C1 are −0.21, 0.22, −0.21, and 0.14, respectively. So, there are 0.20 electrons transferred from the SWCNT to O_3, and the electrostatic interaction scheme in [a]TS1 is qualitatively the same as that in [a]Complex.

Following the imaginary vibrational mode forward, we found that C1 indeed captures O1 producing the final product ([a]Product) and the outgoing singlet O_2 ($^1\Delta_g$) can be immediately quenched into the triplet O_2 ($^3\Sigma_g^-$) through thermal collisions. The structure of [a]Product is shown in Figure 2c. At this stage, the C1−O1 bond is very strong with a bond length of 1.21 Å, close to a typical carbonylic C=O double bond.

The energies of [a]Complex and [a]TS1 are 5.9 and 0.3 kcal/mol lower than the reactants, respectively. The forward reaction barrier is only 5.6 kcal/mol for [a]Complex, and the effective forward reaction barrier of the overall reaction is very close to zero, only −0.3 kcal/mol. The overall energy released from the reaction is −117.7 kcal/mol. On the basis of the energy profile, the reaction of O_3 with C1 is highly exothermic and facile.

3.1.2. 1,3-DC of O_3 on the C8−C9 Bond (Position 1). The structures of the initial intermediate ([P1]Complex) and transition state ([P1]TS1) are shown in Figure 3a and b. [P1]Complex was reported as a π-complex in previous matrix spectroscopic and theoretical studies of ozonization of certain alkenes.[48] The

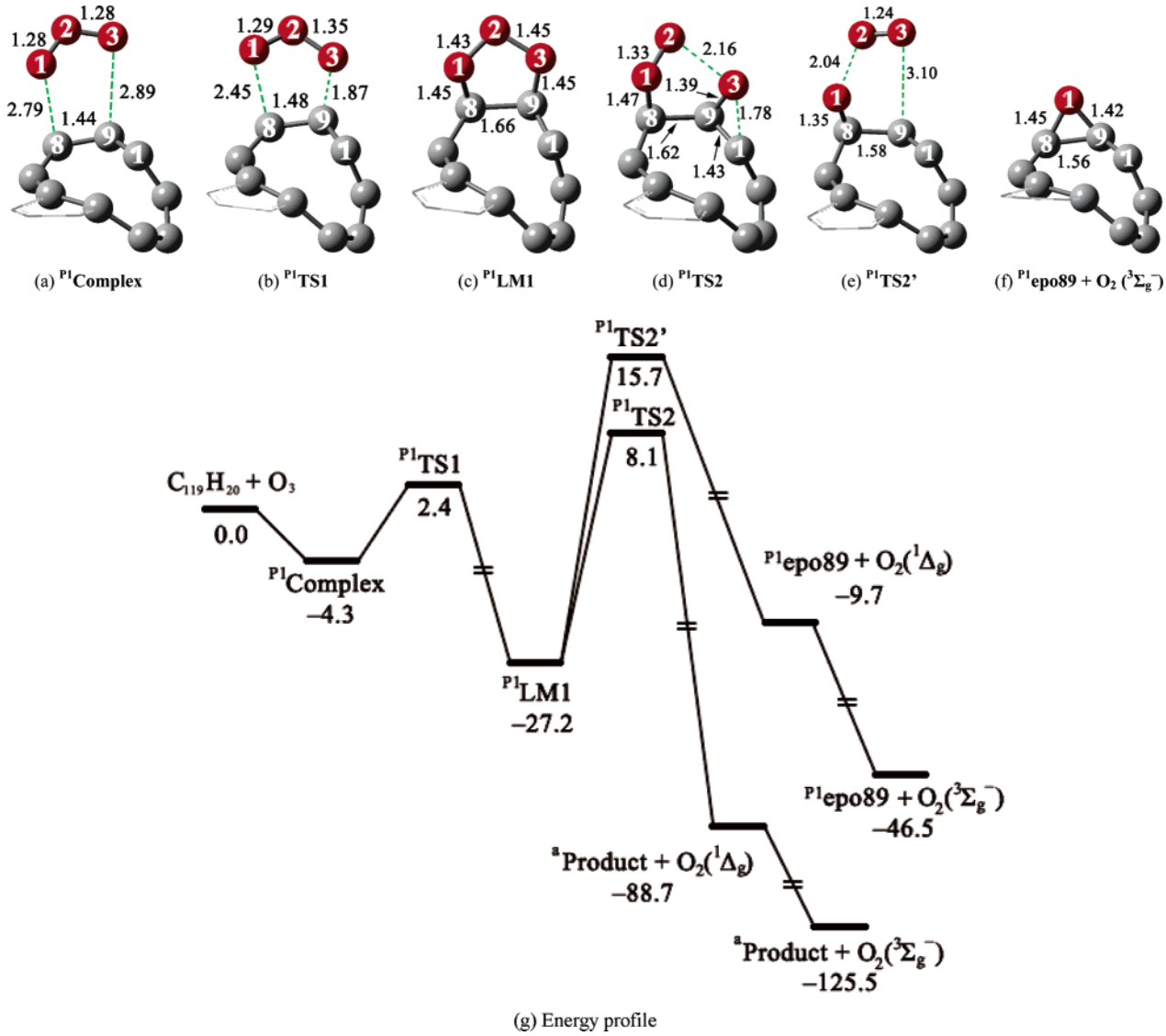

Figure 3. Geometries of the transition states, the intermediates, and the final product of the 1,3-DC of O_3 on the C8−C9 bond (position 1) on the nine-membered ring of $C_{119}H_{20}$. The units of energy and bond length are kcal/mol and Å, respectively. The oxygen atoms are in red.

complex is stabilized by the interaction of the π-type HOMO and LUMO on alkenes and O_3. ^{P1}Complex is 4.3 kcal/mol more stable than the reactants, whereas ^{P1}TS1 lays 2.4 kcal/mol above the reactants. In ^{P1}TS1, the lengths of the C8−O1 and C9−O3 bonds are 2.45 and 1.87 Å, respectively. This indicates that the 1,3-DC of O_3 on C8−C9 follows an asynchronous pattern. In the first intermediate ^{P1}LM1 (Figure 3c), the C8−C9 bond length is 1.66 Å, longer than those of ^{P1}Complex (1.44 Å) and ^{P1}TS1 (1.48 Å), due to the rehybridization of C8 and C9 from sp^2 to sp^3. The binding energy of ^{P1}LM1 is −27.2 kcal/mol (relative to the reactants): the 1,3-DC of O_3 on C8−C9 is exothermic.

We also explored the forward decomposition of ^{P1}LM1. Two different pathways were found. In the first pathway, the system climbs through the transition state ^{P1}TS2 (Figure 3d), by breaking the O2−O3 bond (2.16 Å) and forming the C1−O3 bond (1.78 Å), with an activation barrier 35.3 kcal/mol. After overcoming ^{P1}TS2, O1 and O2 dissociate as a singlet O_2, the C9−O3 bond breaks, and O3 forms a carbonylic C=O double bond with C1 and yields the same product ^{a}Product as in the reaction of O_3 on C1.

The second decomposition pathway goes through another transition state ^{P1}TS2′ (Figure 3e) and forms an epoxy adduct ^{P1}epo89 (Figure 3f). The imaginary vibrational mode clearly shows the breaking of the O1−O2 and C9−O3 bonds. The activation barrier from ^{P1}LM1 to ^{P1}TS2′ is 42.9 kcal/mol, which is 7.6 kcal/mol higher than that of the first decomposition pathway. In contrast to the high exothermicity of the first decomposition pathway (−61.5 kcal/mol relative to ^{P1}LM1), the second decomposition pathway is endothermic (17.5 kcal/mol with respect to ^{P1}LM1). Therefore, the first decomposition pathway is kinetically and thermodynamically much more favorable than the second decomposition pathway.

However, the high reaction barrier (35.3 kcal/mol) from ^{P1}LM1 to the products makes this reaction pathway uncompetitive to the dissociation pathway on the active atom.

3.1.3. 1,3-DC of O_3 on the C6−C7 Bond (Position 2). The structures of ^{P2}Complex, ^{P2}TS1, and ^{P2}LM1 are shown in Figure 4a−c. ^{P2}Complex is also a π-complex according to its structure. The imaginary frequency mode of ^{P2}TS1 mainly shows the attack of O1 on C6 and the stretching of the C5−C6 bond. In the primary ozonide ^{P2}LM1, the C5−C6 bond (1.72 Å) is nearly broken. With respect to the energy of the reactants, ^{P2}Complex lays 4.5 kcal/mol lower, whereas ^{P2}TS1 stays 6.4 kcal/mol higher. Thus, the forward reaction barrier from ^{P2}Complex is 10.9 kcal/mol, which is 5.3 kcal/mol higher than that of the reaction on C1. The binding energy of ^{P2}LM1 is

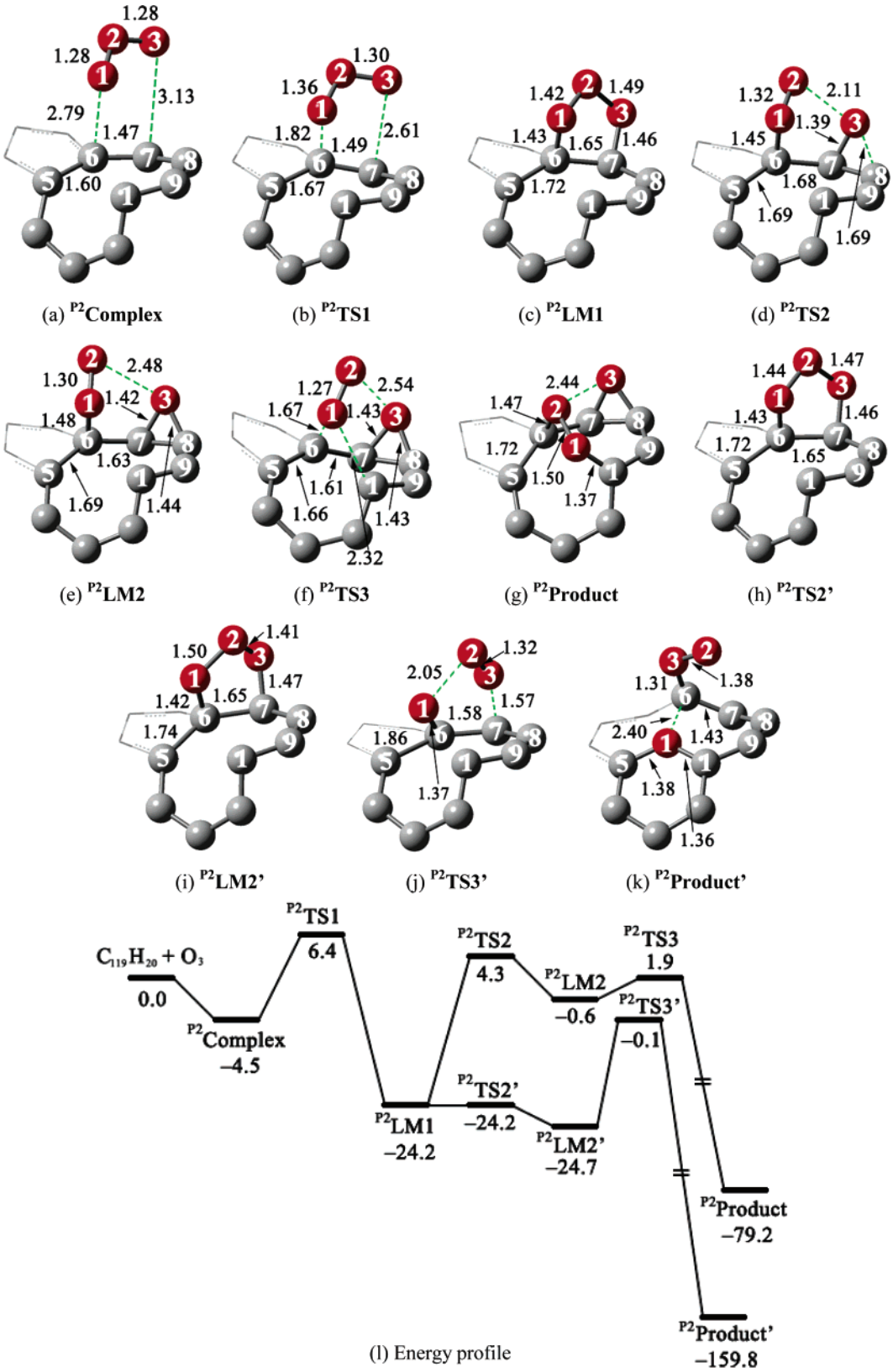

Figure 4. Geometries of the transition states, the intermediates, and the final product of the 1,3-DC of O_3 on the C6−C7 bond (position 2) on the nine-membered ring of $C_{119}H_{20}$. The units of energy and bond length are kcal/mol and Å, respectively. The oxygen atoms are in red.

−24.2 kcal/mol: the 1,3-DC of O_3 on C6−C7 is also exothermic.

Two different decomposition or isomerization pathways of ^{P2}LM1 were explored. The first pathway needs to overcome a 28.5 kcal/mol activation barrier and reaches the transition state ^{P2}TS2 (Figure 4d), in which O3 attacks C8 and breaks the O2−O3 bond. After passing ^{P2}TS2, the system relaxes to ^{P2}LM2 (Figure 4e) by releasing nearly 5 kcal/mol of energy. In ^{P2}LM2, O3 forms an epoxy adduct with C7 and C8, and C6−O1 elongates slightly. ^{P2}LM2 is 23.6 kcal/mol less stable than ^{P2}LM1. ^{P2}LM2 can isomerize to ^{P2}Product (Figure 4g) through another transition state, ^{P2}TS3 (Figure 4f), by

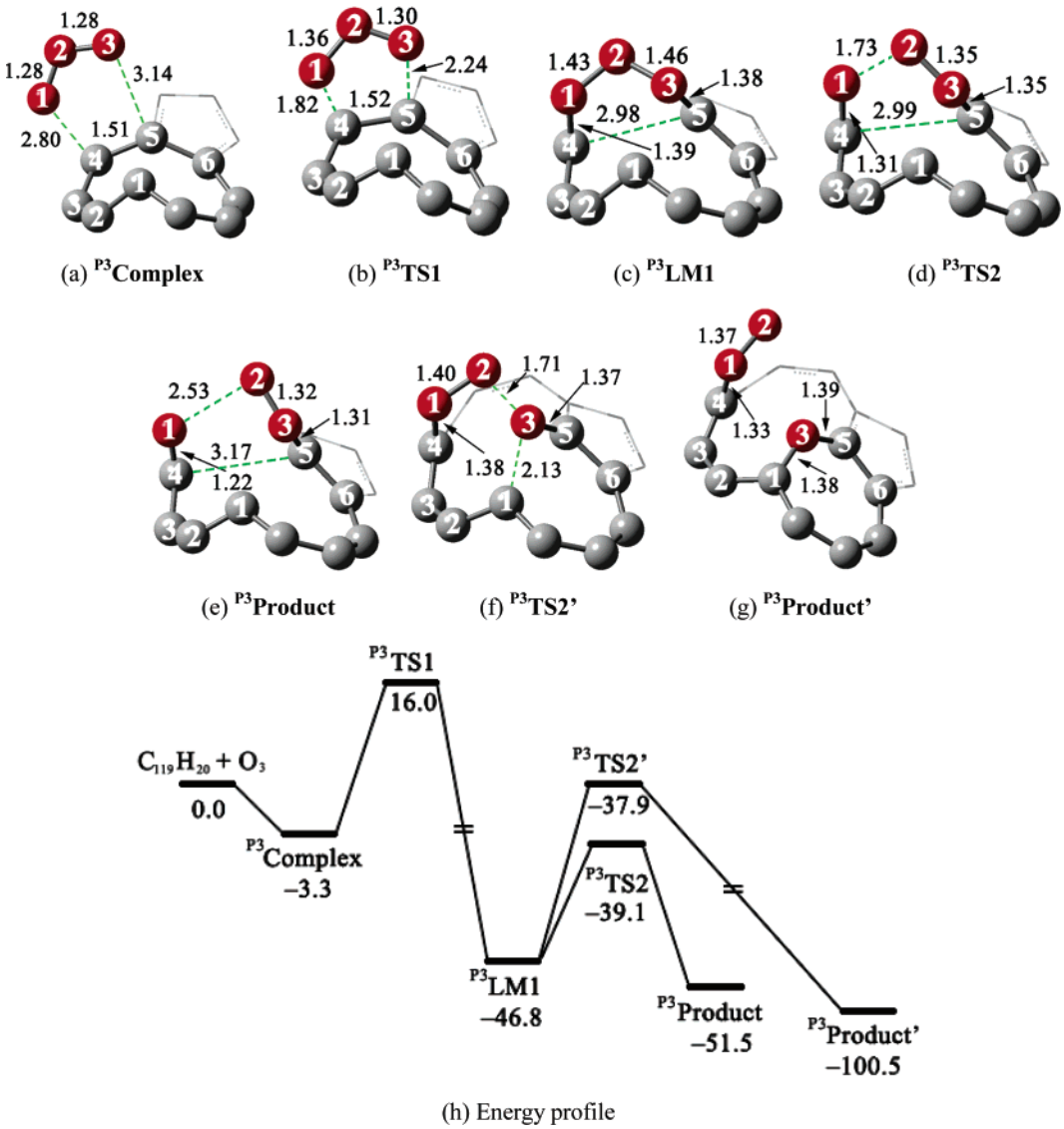

Figure 5. Geometries of the transition states, the intermediates, and the final product of the 1,3-DC of O_3 on the C4−C5 bond (position 3) on the nine-membered ring of $C_{119}H_{20}$. The units of energy and bond length are kcal/mol and Å, respectively. The oxygen atoms are in red.

overcoming a small barrier of 2.5 kcal/mol. In ^{P2}TS3, O1 begins to migrate from C6 to C1. In ^{P2}Product, O1 forms a bond with C1 and O2 forms a bond with C6: O1 and O2 thus coalesce into a bridge between C6 and C1. ^{P2}Product is 79.2 kcal/mol more stable than the reactants.

Another isomerization pathway of ^{P2}LM1 goes through the transition state ^{P2}TS2′ (Figure 4h), in which O1, O2, O3, C6, and C7 are almost in the same plane. The imaginary vibrational mode of ^{P2}TS2′ clearly shows the swinging motion of O2 about the O1−O3−C6−C7 plane. There is virtually no energy cost in going from ^{P2}LM1 to ^{P2}TS2′. After passing ^{P2}TS2′, the system goes to the endoprimary ozonide ^{P2}LM2′ (Figure 4i), whose energy is only 0.5 kcal/mol lower than that of the exoprimary ozonide ^{P2}LM1. The isomerization continues moving forward to overcome a 24.8 kcal/mol barrier and reaches ^{P2}TS3′ (Figure 4j), in which C5−C6 is almost broken (1.86 Å). Here, the imaginary vibrational mode shows the breaking of the O3−C7 and O1−O2 bonds and the attack of O1 to C5. Once overcoming this barrier, the system yields the final product ^{P2}Product′ (Figure 4k), which is 159.8 kcal/mol more stable than the reactants.

However, the 24.6 kcal/mol reaction barrier from ^{P2}LM2′ to the final products renders this pathway unfavorable compared to the dissociation on the active atom.

3.1.4. 1,3-DC of O_3 on the C4−C5 Bond (Position 3). The structures of ^{P3}Complex, ^{P3}TS1, and ^{P3}LM1 are shown in Figure 5a−c. ^{P3}Complex is also a π-complex according to its structure. The imaginary vibrational mode of ^{P3}TS1 clearly indicates the concerted attack of O1 to C4 and O3 to C5 and shows the stretching of the C4−C5 bond. The reaction barrier for the 1,3-DC on C4−C5 is 19.3 kcal/mol. After overcoming this barrier, the system goes to ^{P3}LM1, which is not a primary ozonide. In ^{P3}LM1, the C4−C5 bond (2.98 Å) is totally broken and O1, O2, and O3 form a bridge between C4 and C5. ^{P3}LM1 is 46.8 kcal/mol below the energy of the reactants. It is thermodynamically more stable than the primary ozonides ^{P1}LM1 and ^{P2}LM1.

Two isomerization pathways of ^{P3}LM1 were found. The first one goes through ^{P3}TS2 (Figure 5d), by breaking the O1−O2 bond with a barrier of only 7.7 kcal/mol. After crossing ^{P3}TS2, the system goes to ^{P3}Product (Figure 5e), which is 51.5 kcal/mol more stable than the reactants. Another pathway goes through ^{P3}TS2′ (Figure 5f), in which O3 attacks C1 and simultaneously breaks the bond with O2 with a barrier of only 8.9 kcal/mol. The product, ^{P3}Product′, is shown in Figure 5g, in which O3 bridges C1 and C5, and it is 100.5 kcal/mol more stable than the reactants.

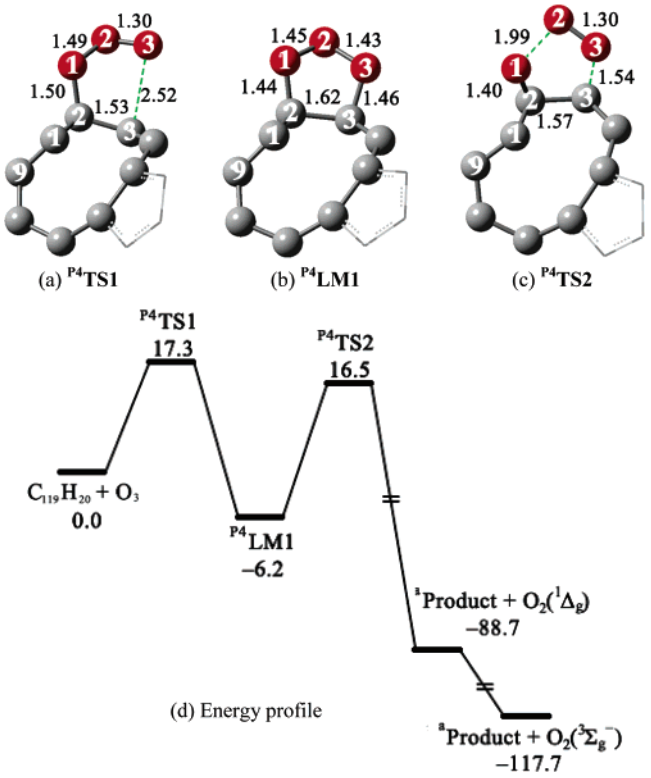

Figure 6. Geometries of the transition states, the intermediates, and the final product of the 1,3-DC of O_3 on the C2−C3 bond (position 4) on the nine-membered ring of $C_{119}H_{20}$. The units of energy and bond length are kcal/mol and Å, respectively. The oxygen atoms are in red.

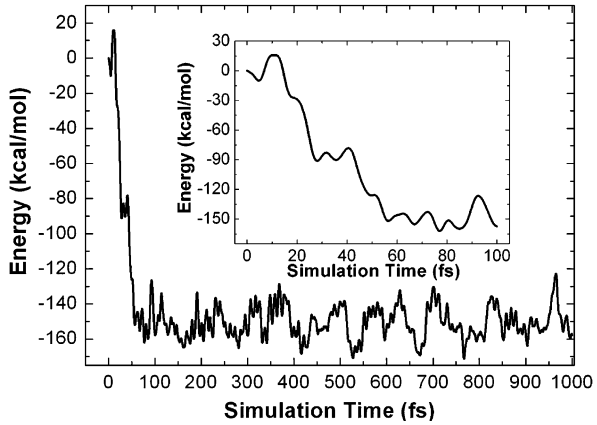

Figure 7. Relative potential energy (in kcal/mol) for the system during the ADMP simulation of 1 ps at 300 K. The insert is the relative potential energy for the first 100 fs.

Despite the exothermicity of this reaction pathway, the first reaction barrier from ^{P3}Complex to ^{P3}LM1 is much higher than the corresponding reaction barrier from ^{a}Complex to ^{a}TS1.

3.1.5. Reaction of O_3 on the C2−C3 Bond (Position 4). The structures of ^{P4}TS1 and ^{P4}LM1 are shown in Figure 6a and b. We did not find a π-complex for the reaction on the C2−C3 bond. In ^{P4}TS1, the O1−C2 bond is 1.50 Å long, which is much shorter than those in the previous initial-reaction transition states. The reaction barrier is 17.3 kcal/mol. The primary ozonide ^{P4}LM1 is only 6.2 kcal/mol more stable than the reactants and is the least stable primary ozonide we have found.

We also found a dissociation pathway for ^{P4}LM1 with an activation barrier of 23.5 kcal/mol. The system goes through ^{P4}TS2 (Figure 6c), in which O1 begins to break the bond with O_2 and to attack C1, concurrently, and O2−O3 tends to leave as the singlet O_2. After overcoming ^{P4}TS2, O2−O3 indeed dissociates from the system and O1 migrates from C2 to C1, yielding the same final product (^{a}Product) as that in the reaction on C1.

In comparison with the initial reaction barrier of the dissociation at the active carbon atom, this initial reaction barrier is too high for the system to reach ^{P4}LM1.

3.2. Ab initio Molecular Dynamics Studies. Static quantum mechanical studies have investigated five different reaction positions of O_3 on the nine-membered ring of the 5-1DB defect site. After comparing all the reaction pathways, we can conclude that the reaction of O_3 on the active carbon atom C1 is most probable, because it is a one-step reaction with the lowest initial attacking barrier. This reaction pathway is kinetically much more favorable than the other ones.

To confirm our assessment from the static quantum mechanical studies of the reactions of O_3 around the 5-1DB defect, we have carried out ADMP-based AIMD simulations at 300 K. Initially, we placed an O_3 molecule above the center of nine-membered ring so that all the reactive sites around the 5-1DB defect have an equal chance to interact with the incoming O_3 molecule. Our dynamical simulation results confirm the spontaneous dissociation of O_3 on C1 to be the most probable reaction process, whose animated reaction trajectory is available in the Supporting Information.

The change of potential energy of the system during the simulations is shown in Figure 7. In less than 50 fs, the system quickly overcomes an ca. 20 kcal/mol barrier and releases a large amount of heat (about 160 kcal/mol), during which one oxygen atom is captured by the active carbon atom C1, forming a carbonylic C═O bond, and the other two oxygen atoms leave as O_2. This mechanism is consistent with the scenario from the static quantum mechanical study discussed above, despite the differences in the energetics because of the different methods used for the lower layer of the two-layered ONIOM model.

4. Conclusion

In conclusion, we have investigated the reactions of O_3 with the 5-1DB defect on the (5,5) SWCNT by static quantum mechanical and ADMP-based AIMD methods within a two-layered ONIOM model. Different pathways on the five possible reactive positions of the nine-membered ring of the 5-1DB defect were explored. The most favorable reaction takes place on the active carbon atom, through a one-step process, in which the active carbon atom captures an oxygen atom from O_3 and the remaining two oxygen atoms dissociate away as a singlet O_2. The other four reaction pathways follow the standard 1,3-dipolar cycloaddition mechanism. Our AIMD dynamical simulation at 300 K indicates the fast spontaneous dissociation of O_3 on the 5-1DB defect. The high exothermicity and the low reaction barrier of this dissociation reaction suggest that it is thermally and kinetically very favorable.

Acknowledgment. The financial support from the Natural Sciences and Engineering Research Council (NSERC) of Canada is gratefully acknowledged. WestGrid and C-HORSE have provided the necessary computational resources. L.V.L. gratefully acknowledges the Gladys Estella Laird and the Charles A. McDowell fellowships from the Department of Chemistry at the University of British Columbia. W.Q.T. received a postdoctoral fellowship from the Japan Society for the Promotion of Science (JSPS) and thanks Professor Yuriko Aoki at Kyushu University for her hospitality.

Supporting Information Available: Clip of the AIMD simulations for O_3 reacting with the 5-1DB defect of the (5,5)

SWCNT. This material is available free of charge via the Internet at http://pubs.acs.org.

References and Notes

(1) Iijima S.; Ichihashi, T. *Nature* **1993**, *363*, 603.

(2) Kong, J.; Franklin, N. R.; Zhou, C. W.; Chapline, M. G.; Peng, S.; Cho, K. J.; Dai, H. J. *Science* **2000**, *287*, 622.

(3) Liu C.; Fan, Y. Y.; Liu, M.; Cong, H. T.; Cheng, H. M.; Dresselhaus, M. S. *Science* **1999**, *286*, 1127.

(4) Zhou, O.; Shimoda, H.; Gao, B.; Oh, S.; Fleming, L.; Yue, G. *Acc. Chem. Res.* **2002**, *35*, 1045.

(5) Ebbsen, T. W. *Carbon Nanotubes: Preparation and Properties*; CRC Press: Boca Raton, FL, 1997.

(6) Tsang, S. C.; Harris, P. J. F.; Green, M. L. H. *Nature* **1993**, *362*, 520.

(7) Ajayan, P. M.; Ebbesen, T. W.; Ichihashi, T.; Iijima, S.; Tanigaki, K.; Hiura, H. *Nature* **1993**, *362*, 522.

(8) Liu, J.; Rinzler, A. G.; Dai, H.; Hafner, J. H.; Bradley, R. K.; Boul, P. J.; Lu, A.; Iverson, T.; Shelimov, K.; Huffman, C. B.; Rodriguez-Macias, F.; Shon, Y.-S.; Lee, T. R.; Colbert, D. T.; Smalley, R. E. *Science* **1998**, *280*, 1253.

(9) Mawhinney, D. B.; Naumenko, V.; Kuznetsova, A.; Yates, J. T.; Liu, J.; Smalley, R. E. *J. Am. Chem. Soc.* **2000**, *122*, 2383.

(10) Byl, O.; Kondratyuk, P.; Forth, S. T.; FitzGerald, S. A.; Chen L.; Johnson, J. K.; Yates, J. T. *J. Am. Chem. Soc.* **2003**, *125*, 5889.

(11) Mawhinney, D. B.; Naumenko, V.; Kuznetsova, A.; Yates, J. T.; Liu, J.; Smalley, R. E. *Chem. Phys. Lett.* **2000**, *324*, 213.

(12) Kuznetsova, A.; Popova, I.; Yates, J. T.; Bronikowski, M. J.; Huffman, C. B.; Liu, J.; Smalley, R. E.; Hwu, H. H.; Chen, J. G. G. *J. Am. Chem. Soc.* **2001**, *123*, 10699.

(13) Kuznetsova, A.; Mawhinney, D. B.; Naumenko, V.; Yates, J. T.; Liu, J.; Smalley, R. E. *Chem. Phys. Lett.* **2000**, *321*, 292.

(14) Niyogi, S.; Hamon, M. A.; Hu, H.; Zhao, B.; Bhowmik, P.; Sen, R.; Itkis, M. E.; Haddon, R. C. *Acc. Chem. Res.* **2002**, *35*, 1105.

(15) Criegee, R. *Angew. Chem., Int. Ed. Engl.* **1975**, *14*, 745.

(16) Shang, Z.; Pan, Y.; Cai, Z.; Zhao, X.; Tang, A. *J. Phys. Chem. A* **2000**, *104*, 1915.

(17) Lu, X.; Zhang, L.; Xu, X.; Wang, N.; Zhang, Q. *J. Phys. Chem. B* **2002**, *106*, 2136.

(18) Yim W. L.; Liu, Z. F. *Chem. Phys. Lett.* **2004**, *398*, 297.

(19) Picozzi, S.; Santucci, S.; Lozzi, L.; Cantalini, C.; Baratto, C.; Sberveglieri, G.; Armentan, I.; Kenny, J. M.; Valentini, L.; Delley, B. *J. Vac. Sci. Technol., A* **2004**, *22*, 1466.

(20) Picozzi, S.; Santucci, S.; Lozzi, L.; Valentini, L.; Delley, B. *J. Chem. Phys.* **2004**, *120*, 7147.

(21) Lu, X.; Chen, Z.; Schleyer, P. V. R. *J. Am. Chem. Soc*. **2005**, *127*, 20.

(22) (a) Kiang, C.-H.; Goddard, W. A., III; Beyers, R.; Bethune, D. S. *J. Phys. Chem.* **1996**, *100*, 3749. (b) Zhu, Y.; Yi, T.; Zheng, B.; Cao, L. *Appl. Surf. Sci.* **1999**, *137*, 83.

(23) Ajayan, P. M.; Ravikumar, V.; Charlier, J.-C. *Phys. Rev. Lett.* **1998**, *81*, 1437.

(24) Lu, A. J.; Pan, B. C. *Phys. Rev. Lett.* **2004**, *92*, 105504.

(25) Tian, W. Q.; Liu, L. V.; Wang, Y. A. Electronic Properties and Reactivity of the Pt-Doped Carbon Nanotubes. *Phys. Chem. Chem. Phys.*, published online May 17, http://dx.doi.org/10.1039/b604032m.

(26) Liu, L. V.; Tian, W. Q.; Wang, Y. A. *J. Phys. Chem. B* **2006**, *110*, 1999.

(27) Tian, W. Q.; Liu, L. V.; Wang, Y. A. In *Handbook of Theoretical and Computational Nanotechnology*; Rieth, M., Schommers, W., Eds.; American Scientific: Valencia, CA, 2006; Chapter 117.

(28) Fagan, S. B.; da Silva, L. B.; Mota, R. *Nano Lett.* **2003**, *3*, 289.

(29) Mielke, S. L.; Troya, D.; Zhang, S.; Li, J. L.; Xiao, S. P.; Car, R.; Ruoff, R. S.; Schatz, G. C.; Belytschko, T. *Chem. Phys. Lett.* **2004**, *390*, 413.

(30) Srivastava, D.; Menon, M.; Daraio, C.; Jin, S.; Sadanadan, B.; Rao, A. M. *Phys. Rev. B* **2004**, *69*, 153414.

(31) Hashimoto, A.; Suenaga, K.; Gloter, A.; Urita, K.; Iijima, S. *Nature* **2004**, *430*, 870.

(32) Urita, K.; Suenaga, K.; Sugai, T.; Shinohara, H.; Iijima, S. *Phys. Rev. Lett.* **2005**, *94*, 155502.

(33) Ziegler, K. J.; Gu, Z.; Peng, H.; Flor, E. L.; Hauge, R. H.; Smalley, R. E. *J. Am. Chem. Soc.* **2005**, *127*, 1541.

(34) Dewar, M. J. S.; Zoebisch, E. G.; Healy, E. F.; Stewart, J. P. P. *J. Am. Chem. Soc.* **1986**, *108*, 5771.

(35) Becke, A. D. *J. Chem. Phys.* **1993,** *98*, 5648.

(36) Lee, C.; Yang, W.; Parr, R. G. *Phys. Rev. A* **1988**, *37*, 785.

(37) Liu, L. V.; Tian, W. Q.; Wang, Y. A. Ab Initio Studies of the Vacancy Defected Fullerenes and Single-Walled Carbon Nanotubes. *J. Chem. Phys.* **2006**, submitted for publication.

(38) Maseras F.; Morokuma. K. *J. Comput. Chem.* **1995**, *16*, 1170.

(39) Glendening, E. D.; Carpenter, A. E.; Weinhold F. *NBO Version 3.1*; 1995. Reed, A. E.; Curtiss, L. A.; Weinhold, F. *Chem. Rev.* **1988**, *88*, 899.

(40) Frisch, M. J.; et al. *Gaussian 03*, revision B.05; Gaussian, Inc.: Pittsburgh, PA, 2003.

(41) (a) Parisel, O.; Ellinger, Y.; Giessner-Prettre, C. *Chem. Phys. Lett.* **1996**, *250*, 178. (b) Garavelli, M.; Bernardi, F.; Olivucci, M.; Robb, M. A. *J. Am. Chem. Soc.* **1998**, *120*, 10210.

(42) Schlegel, H. B.; Millam, J. M.; Iyengar, S. S.; Voth, G. A.; Daniels, A. D.; Scuseria, G. E.; Frisch, M. J. *J. Chem. Phys.* **2001**, *114*, 9758.

(43) Iyengar, S. S.; Schlegel, H. B.; Millam, J. M.; Voth, G. A.; Scuseria, G. E.; Frisch, M. J. *J. Chem. Phys.* **2001**, *115*, 10291.

(44) Schlegel, H. B.; Iyengar, S. S.; Li, X.; Millam, J. M.; Voth, G. A.; Scuseria, G. E.; Frisch, M. J. *J. Chem. Phys.* **2002**, *117*, 8694.

(45) Tian, W. Q.; Wang, Y. A. *J. Chem. Theory Comput.* **2005**, *1*, 353.

(46) Rega, N.; Iyengar, S. S.; Voth, G. A.; Schlegel, H. B.; Vreven, T.; Frisch, M. J. *J. Phys. Chem. B* **2004**, *108*, 4210.

(47) Rappe, A. K.; Casewit, C. J.; Colwell, K. S.; Goddard, W. A., III; Skiff, W. M. *J. Am. Chem. Soc.* **1992**, *114*, 10024.

(48) (a) Kohlmiller, C. K.; Andrews, L. *J. Am. Chem. Soc.* **1981**, *103*, 2578. (b) McKee, M. L.; Rohlfing, C. M. *J. Am. Chem. Soc.* **1989**, *111*, 2497.